

## Article

# XPS and NEXAFS Characterization of Mg/Zn and Mn Codoped Bismuth Tantalate Pyrochlores

Nadezhda A. Zhuk <sup>1,\*</sup>, Boris A. Makeev <sup>2</sup>, Aleksandra V. Koroleva <sup>3</sup>, Aleksey M. Lebedev <sup>4</sup>, Olga V. Petrova <sup>5</sup>, Sergey V. Nekipelov <sup>5</sup> and Viktor N. Sivkov <sup>5</sup>

<sup>1</sup> Institute of Natural Sciences, Syktyvkar State University, Oktyabrsky Prospect, 55, Syktyvkar 167001, Russia

<sup>2</sup> Institute of Geology of the Komi Science Center UB RAS, Pervomaiskaya St. 48, Syktyvkar 167982, Russia; makboris@mail.ru

<sup>3</sup> Research Park, Saint Petersburg State University, Saint Petersburg 199034, Russia; dalika@inbox.ru

<sup>4</sup> National Research Center, Kurchatov Institute, 1 Akad. Kurchatova Sq., Moscow 123182, Russia; lebedev.alex.m@gmail.com

<sup>5</sup> Institute of Physics and Mathematics, Komi Science Centre, Ural Branch of the Russian Academy of Sciences, Syktyvkar 167982, Russia; teiou@mail.ru (O.V.P.); nekipelovsv@mail.ru (S.V.N.); sivkovvn@mail.ru (V.N.S.)

\* Correspondence: nzhuck@mail.ru

**Abstract:** Two series of the bismuth tantalate pyrochlore samples, codoped with Mg,Mn and Zn,Mn, were synthesized via solid-phase reaction. It was established that the  $\text{Bi}_2\text{Mg}(\text{Zn})_x\text{Mn}_{1-x}\text{Ta}_2\text{O}_{9-\Delta}$  ( $x = 0.3; 0.5; 0.7$ ) samples contain the main phase of cubic pyrochlore (sp. gr. Fd-3m) and an admixture of triclinic  $\text{BiTaO}_4$  (sp. gr. P-1). In both sets, the amount of  $\text{BiTaO}_4$  is proportional to the amount of manganese doping, however, zinc-containing samples have a higher level of impurities than magnesium-containing ones. The unit cell parameter of the Zn,Mn codoped bismuth tantalate phase increases with an increasing content of zinc ions in the samples from 10.4895(5) ( $x = 0.3$ ) to 10.5325(5) Å ( $x = 0.7$ ). The unit cell parameter of Mg,Mn codoped bismuth tantalate pyrochlores increases uniformly with an increasing index  $x(\text{Mg})$  from 10.4970(8) at  $x = 0.3$  to 10.5248(8) Å at  $x = 0.7$ , according to the Vegard rule. The NEXAFS and XPS data showed that the ions were found to have oxidation states of Bi(+3), Ta(+5), Zn(+2) and Mg(+2). In the Ta 4f XPS spectrum of both series of samples, a low energy shift of the absorption band characteristic of tantalum ions with an effective charge of (+5- $\delta$ ) was observed. The XPS spectra of Bi4f7/2 and Bi4f5/2 also show a shift of bands towards lower energies which is attributed to the presence of some low-charge ions of transition elements in the bismuth position. The NEXAFS spectroscopy data showed that manganese ions in both series of samples have predominantly 2+ and 3+ oxidation states. XPS data indicate that in zinc-containing preparations the proportion of oxidized manganese ions is higher than in magnesium-containing ones.

**Keywords:** pyrochlore; Zn; Mg; Mn doping;  $\text{BiTaO}_4$ ; XPS and NEXAFS spectroscopy



**Citation:** Zhuk, N.A.; Makeev, B.A.; Koroleva, A.V.; Lebedev, A.M.; Petrova, O.V.; Nekipelov, S.V.; Sivkov, V.N. XPS and NEXAFS Characterization of Mg/Zn and Mn Codoped Bismuth Tantalate Pyrochlores. *Inorganics* **2024**, *12*, 74. <https://doi.org/10.3390/inorganics12030074>

Academic Editor: Antonino Gulino

Received: 23 December 2023

Revised: 3 February 2024

Accepted: 7 February 2024

Published: 29 February 2024



**Copyright:** © 2024 by the authors. Licensee MDPI, Basel, Switzerland. This article is an open access article distributed under the terms and conditions of the Creative Commons Attribution (CC BY) license (<https://creativecommons.org/licenses/by/4.0/>).

## 1. Introduction

In 2026, it will be 200 years since the first information was obtained about natural minerals of the niobium group  $(\text{Na,Ca})_2\text{Nb}_2\text{O}_6(\text{OH,F})$ , which were called pyrochlore from the Greek words “fire” and “green” due to their green color when heated [1]. Pyrochlores are an important class of materials in various technological applications due to a wide range of practically useful properties, including metallic and ionic conductivity, superconducting and ferroelectric properties [2,3]. They exhibit ferro- and antiferromagnetism, magnetoresistance and a spin glass state [4–6]. Materials based on pyrochlores are used in solid-state devices as thin-film resistors, thermistors, communication elements and photocatalysts, and are used as components of ceramic molds for radioactive waste. Due to their excellent dielectric properties, their ability to regulate dielectric properties using an electric field, their low sintering temperature and chemical compatibility with low-melting Ag and Cu

conductors, oxide pyrochlores are promising as dielectrics for multilayer ceramic capacitors, tunable microwave dielectric components, resonators, and devices for microwave applications [7–9].

The general formula of oxide pyrochlores  $A_2B_2O_7$  describes a large family of compounds isostructural with the mineral pyrochlore. In the crystal structure of pyrochlore, two cationic sublattices with the anticristobalite structure  $A_2O'$  and the octahedral  $B_2O_6$  are distinguished. The positions of cations A with octaoxygen coordination are occupied by large ions ( $Ca^{2+}$ ,  $Bi^{3+}$ ). The three-dimensional framework of  $B_2O_6$  is formed by  $[BO_6]$  octahedra connected at the vertices, in the positions of which cations with a smaller ionic radius ( $Ti^{4+}$ ,  $Ta^{5+}$ ) are located [10,11]. There are known cases of mixed pyrochlores with three or more types of cations located at two nonequivalent cation positions A and B. These include pyrochlores based on bismuth tantalate, doped with ions of 3 elements [12–14]. Taking into account the polarization properties of these ions and the proximity of their radii to the ionic radius of Ta(V), it is logical to assume their distribution in the octahedral positions of tantalum ions. However, as studies by many scientists have shown [15,16], depending on the chemical nature, a small fraction of transition element ions replaces the Bi(III) positions. Apparently, the reason for this is the tension of the octahedral framework due to the introduction of incommensurate and heterovalent dopant ions ( $Zn^{2+}$ ,  $Mn^{2+}$ ,  $Co^{2+}$ ,  $Cu^+$ ) in relation to Ta(V) ions, as well as the preference of some of them for tetrahedral coordination. Such doping options lead to the formation of a pyrochlore structure deficient in A cations, as is observed for bismuth-containing pyrochlores and is the reason for the relaxation properties of oxide ceramics [12,17]. Currently, almost all pyrochlores based on bismuth tantalate containing 3 ions (Cr, Fe, Co, Ni, Cu, Zn) are known and studied [18–27]. Due to their excellent dielectric properties, such pyrochlores are promising as multilayer ceramic capacitors, resistors, resonators, sensors and microwave filters. It has been established that moderate values of dielectric constant  $\sim 78$ – $92$  and dielectric loss  $\sim 10^{-1}$  at  $30^\circ C$  and 1 MHz are exhibited by iron-containing pyrochlores  $Bi_{3.36}Fe_{2.08+x}Ta_{2.56-x}O_{14.56-x}$  ( $-0.32 \leq x \leq 0.48$ ) [27]. Magnesium-containing pyrochlores  $Bi_{3+5/2x}Mg_{2-x}Ta_{3-3/2x}O_{14-x}$  ( $0.12 \leq x \leq 0.22$ ) are characterized by comparable values of  $\epsilon \sim 70$ – $85$  and low dielectric loss tangent  $\delta \sim 10^{-3}$  at 1 MHz and  $30^\circ C$  [28,29]. For zinc-containing pyrochlores  $Bi_{1.5}ZnTa_{1.5}O_7$ , the dielectric constant under standard conditions does not exceed 60 [25,26]. We have not found any information on manganese-containing pyrochlores based on bismuth tantalate. There is one known work [15] devoted to the study of analog pyrochlores in the  $Bi_2O_3$ - $Mn_2O_3$ - $Nb_2O_5$  system. The authors of the article established that a significant concentration region of bismuth-deficient manganese-containing pyrochlores is formed in the system, in which 14–30% of the A-positions are occupied by  $Mn^{2+}$  ions. As the authors of [15] showed, X-ray powder diffraction data confirmed that all Bi–Mn–Nb–O pyrochlores form with structural displacements, as found for the analogous pyrochlores with Mn replaced by Zn, Fe, or Co. According to [15], the displacive disorder is crystallographically analogous to that reported for  $Bi_{1.5}Zn_{0.92}Nb_{1.5}O_{6.92}$ , which has a similar concentration of small B-type ions on the A-sites. EELS spectra of manganese-containing pyrochlores showed the presence of  $Mn^{2+}$  and  $Mn^{3+}$  ions. As is known, manganese in high-temperature ceramics can have a complex ionic composition (the oxidation state of manganese varies from 2+ to 4+), which affects the physicochemical properties of the ceramics. The ionic state of manganese is influenced by many variable factors, among which is the symmetry and strength of the crystal field, and the nature of the ligands; distortions and the size of the coordination polyhedron are particularly prominent. Studies have shown that the combined use of X-ray spectroscopy methods (XPS, NEXAFS) make it possible to most accurately determine the ionic composition of complex oxides [30]. As part of our work, we studied the electronic state of manganese ions in Mg(Zn), Mn codoped bismuth tantalate pyrochlores using NEXAFS and XPS spectroscopy. The influence of zinc and magnesium and the degree of substitution of Ta(V) ions on the proportion of oxidized manganese ions in pyrochlores has been established.

## 2. Experimental Part

$\text{Bi}_2\text{Zn}(\text{Mg})_x\text{Mn}_{1-x}\text{Ta}_2\text{O}_{9.5-\Delta}$  ( $x = 0.3, 0.5, 0.7$ ) samples were synthesized using the solid-phase reaction method from the oxides  $\text{ZnO}$ ,  $\text{MgO}$ ,  $\text{Bi}_2\text{O}_3$ ,  $\text{Mn}_2\text{O}_3$ ,  $\text{Ta}_2\text{O}_5$ . A finely ground and homogeneous mixture of oxides in stoichiometric quantities was pressed into disk-shaped compacts (diameter 10 mm, thickness 3–4 mm) using a hand press. High-temperature treatment of the samples was carried out in stages, at temperatures of 650, 850, 950, 1050 °C for 15 h at each calcination stage. The phase composition was determined by X-ray phase analysis using a Shimadzu 6000 X-ray diffractometer ( $\text{CuK}\alpha$  radiation). The microstructure and local elemental composition of the samples were studied using scanning electron microscopy and energy-dispersive X-ray spectroscopy (electron scanning microscope Tescan VEGA 3LMN, Japan, energy dispersion spectrometer INCA Energy 450, Japan). XPS studies were carried out using the equipment of the resource center of the Science Park of St. Petersburg State University “Physical methods of surface research.” XPS analysis was performed on a Thermo Scientific ESCALAB 250Xi X-ray spectrometer, Great Britain. An X-ray tube with  $\text{AlK}\alpha$  radiation (1486.6 eV) was used as a source of ionizing radiation. To neutralize the sample charge in the experiments, an ion-electronic charge compensation system was used. All peaks were calibrated relative to the  $\text{C1s}$  peak at 284.6 eV. The processing of experimental data was carried out using the software of the ESCALAB 250Xi spectrometer (Avantage v5.9925, Great Britain). The samples were studied using NEXAFS spectroscopy at the NanoFES station of the KISS synchrotron source at the Kurchatov Institute (Moscow, Russia) [30]. NEXAFS spectra were obtained by recording the total electron yield (TEY) with an energy resolution of 0.5 eV.

## 3. Results and Discussion

### 3.1. Phase Composition of the $\text{Bi}_2\text{Zn}(\text{Mg})_x\text{Mn}_{1-x}\text{Ta}_2\text{O}_{9.5-\Delta}$

The choice of the stoichiometry of ceramic is based on our previous research on the doping of magnesium-containing pyrochlores based on bismuth tantalate with transition 3d elements [21,22]. X-ray phase analysis revealed that samples with the composition  $\text{Bi}_2\text{Zn}_x\text{Mn}_{1-x}\text{Ta}_2\text{O}_{9.5-\Delta}$  ( $x = 0.3\text{--}0.7$ ) are two-phase. In addition to the main cubic phase, they contain triclinic bismuth orthotantalate  $\text{BiTaO}_4$  as an impurity (Figure 1) [31]. The analysis of the reflection extinctions of the cubic phase confirmed that the symmetry of the crystal structure is cubic with the space group  $\text{Fd-}3\text{m}$  [10,11]. The unit cell parameter of cubic pyrochlore in  $\text{Bi}_2\text{Zn}_x\text{Mn}_{1-x}\text{Ta}_2\text{O}_{9.5-\Delta}$  increases uniformly with an increase in the zinc ion content (and a decrease in the manganese ion content) in the samples from 10.4895(5) ( $x = 0.3$ ) to 10.5325(5) Å ( $x = 0.7$ ). In addition, X-ray spectroscopy indicates that the ionic radius of zinc(II) ( $R(\text{Zn(II)})_{\text{c.n-6}} = 0.74$  Å) is smaller than that of Mn(II) ions ( $R(\text{Mn(II)})_{\text{c.n-6}} = 0.83$  Å) present in the samples (Figure 1) [32]. The observed unusual behavior can be explained by several factors. Firstly, the amount of impurity decreases with increasing zinc content, resulting in a higher pyrochlore cell parameter. Secondly, Mn(II) ions occupy bismuth(III) positions, which have a similar ionic radius to bismuth(III) ( $R(\text{Bi(III)})_{\text{c.n-8}} = 1.17$  Å,  $R(\text{Mn(II)})_{\text{c.n-8}} = 0.90$  Å), and do not significantly contribute to the cell parameter. The increase in the cell parameter occurs due to the distribution of large zinc(II) ions into the octahedral positions of tantalum(V) ( $R(\text{Zn(II)})_{\text{c.n-6}} = 0.74$  Å,  $R(\text{Ta(V)})_{\text{c.n-6}} = 0.64$  Å). Quantitative assessment of the bismuth orthotantalate content showed that the impurity content varies from 11.9 ( $x(\text{Zn}) = 0.7$ ) to 20.0 wt.% ( $x = 0.3$ ) and increases with increasing manganese content in the samples. As previously demonstrated [20], the presence of impurities in the samples can be associated with the placement of Mn(II) ions both in the octahedral sublattice of tantalum(V) and the bismuth(III) sublattice, due to the larger size of Mn(II) ions compared to Zn(II). It is probable that most of the relatively large manganese ions are distributed within the octahedral sublattice of tantalum(V) leading to oxygen vacancies and stress in the octahedral framework as a whole. In order to relieve stress in the crystal structure, some manganese(II) ions are placed in the bismuth(III) position. This causes the system to create vacancies in the bismuth sublattice, resulting in the release of the bismuth orthotantalate phase as an impurity [20].

In most cases, the amount of bismuth orthotantalate impurity is typically proportional to the number of 3 ions located in the bismuth position [33]. These ions may include manganese(II) and zinc(II) ions, since they have similar ionic radii ( $R(\text{Zn(II)})_{\text{c.n-8}} = 0.90 \text{ \AA}$ ,  $R(\text{Mn(II)})_{\text{c.n-8}} = 0.96 \text{ \AA}$ ) [32]. Additionally, zinc(II) ions are typically characterized by tetrahedral coordination rather than octahedral. On the other hand, manganese(II) ions have a larger ionic radius than Zn(II). Therefore, considering the change in the cell parameter, it can be assumed that all manganese ions occupy the bismuth position, especially at high values of  $x(\text{Mn})$ . The inset in Figure 1 shows the dependence of the change in the unit cell parameter on the manganese content and the amount of  $\text{BiTaO}_4$  impurity in  $\text{Bi}_2\text{Zn}_x\text{Mn}_{1-x}\text{Ta}_2\text{O}_{9.5-\Delta}$ .

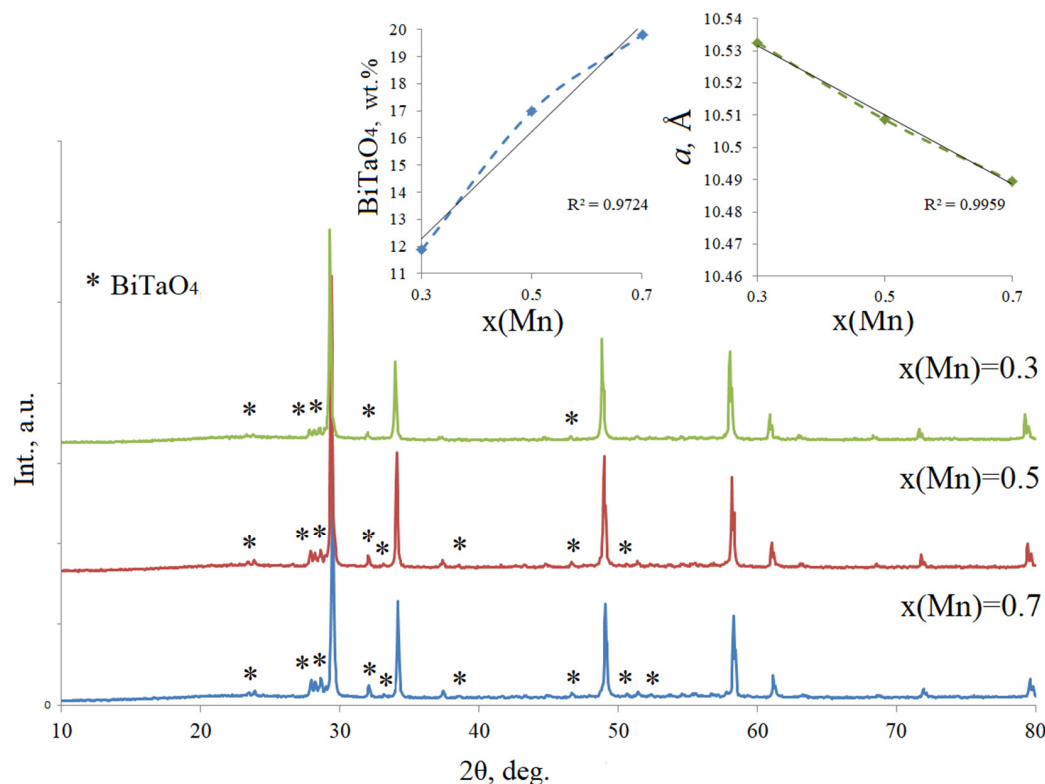


**Figure 1.** X-ray diffraction patterns of samples  $\text{Bi}_2\text{Zn}_x\text{Mn}_{1-x}\text{Ta}_2\text{O}_{9.5-\Delta}$  at different values of the  $x(\text{Mn})$  index. The inset shows the dependence of the amount of  $\text{BiTaO}_4$  impurity and the unit cell parameter of pyrochlore on the  $x(\text{Mn})$  index in the samples.

The magnesium-containing samples of  $\text{Bi}_2\text{Mg}_x\text{Mn}_{1-x}\text{Ta}_2\text{O}_{9.5-\Delta}$  ( $x = 0.3\text{--}0.7$ ) are also two-phase and contain  $\beta\text{-BiTaO}_4$  as an impurity (Figure 2). The amount of bismuth orthotantalate is proportional to the content of manganese ions and varies from 7.9 ( $x(\text{Mn}) = 0.3$ ) to 23.8 wt.% ( $x(\text{Mn}) = 0.7$ ). The proportionality of the impurity amount to the manganese content in the samples may indicate the distribution of some manganese ions in the bismuth position and magnesium ions in the octahedral positions of tantalum(V). This was previously demonstrated in the example of solid solutions  $\text{Bi}_2\text{Mg}_x\text{Mn}_{1-x}\text{Ta}_2\text{O}_{9.5-\Delta}$  (M-Ni, Cr, Fe) [21]. The analysis of the reflection extinctions in the cubic phase confirmed that the symmetry of the crystal structure is cubic and is described by the space group  $\text{Fd-}3\text{m}$ , which is characteristic of cubic pyrochlore [10]. The unit cell parameter of cubic pyrochlore in  $\text{Bi}_2\text{Mg}_x\text{Mn}_{1-x}\text{Ta}_2\text{O}_{9.5-\Delta}$  decreases uniformly with an increase in the content of manganese ions (and a decrease in magnesium ions) in the samples from 10.5248(8) ( $x(\text{Mn}) = 0.3$ ) to 10.4970(8)  $\text{\AA}$  ( $x(\text{Mn}) = 0.7$ ), despite the fact that the ionic radius of magnesium(II) is smaller than that of the Mn(II) ions (Figure 2 insert) ( $R(\text{Mg(II)})_{\text{c.n-6}} = 0.72 \text{ \AA}$ ,  $R(\text{Mn(II)})_{\text{c.n-6}} = 0.83 \text{ \AA}$ ) [32]. This increase is due to the difference in ionic radii between magnesium and tantalum(V) ( $R(\text{Mg(II)})_{\text{c.n-6}} = 0.72 \text{ \AA}$ ,  $R(\text{Ta(V)})_{\text{c.n-6}} = 0.64 \text{ \AA}$ ). When ana-

lyzing the phase composition of  $\text{Bi}_2\text{Mg}(\text{Zn})_x\text{Mn}_{1-x}\text{Ta}_2\text{O}_{9.5-\Delta}$  ( $x = 0.3; 0.5; 0.7$ ) samples, it is noteworthy that the only impurity present in both series with zinc and magnesium is  $\text{BiTaO}_4$ . The amount of impurity increases with increasing manganese content in  $x(\text{Mn})$  samples, which may be due to an increase in the content of large  $\text{Mn}(\text{II})$  ions and their distribution in the  $\text{Bi}(\text{III})$  position. Based on Figure 3a, zinc preparations have a higher impurity level at low concentrations of  $x(\text{Mn}) < 0.5$ , while magnesium pyrochlores have a higher impurity level at higher concentrations of  $x(\text{Mn}) > 0.5$ . There are several reasons for this phenomenon. In accordance with earlier X-ray diffraction studies of magnesium-containing preparations  $\text{Bi}_2\text{Mg}_x\text{M}_{1-x}\text{Ta}_2\text{O}_{9.5-\Delta}$  ( $\text{M}=\text{Ni}, \text{Cr}, \text{Cu}, \text{Fe}$ ) showed the distribution of magnesium ions in the octahedral sublattice, which means that with a combination of  $\text{Mn}/\text{Mg}$  in bismuth positions there will be manganese ions in the entire concentration interval  $x(\text{Mn})$ . In  $\text{Mn}/\text{Zn}$  samples, it was previously noted that both manganese and zinc ions have the potential to occupy bismuth positions. In this regard, the higher amount of impurities in zinc preparations at  $x(\text{Mn}) < 0.5$  can be explained by the fact that with a high content of zinc ions, some of them move to the bismuth position, and with a decrease in zinc ions content, manganese ions are distributed in the bismuth(III) position (II). This statement is supported by the fact that the composition of  $\text{Bi}_2\text{MgTa}_2\text{O}_9$  is a single-phase pyrochlore, while the  $\text{Bi}_2\text{ZnTa}_2\text{O}_9$  sample is a non-single phase with an admixture of  $\text{BiTaO}_4$  in addition to the main pyrochlore phase. It is interesting to note that, despite having the same charge and comparable ionic radii of magnesium and zinc in six and eight coordinate positions ( $R(\text{Bi}(\text{III}))_{\text{c.n-8}} = 1.17 \text{ \AA}$ ,  $R(\text{Mg}(\text{II}))_{\text{c.n-8}} = 0.89 \text{ \AA}$ ,  $R(\text{Zn}(\text{II}))_{\text{c.n-8}} = 0.90 \text{ \AA}$ ), their distribution in the bismuth position is different and zinc ions have a greater tendency to occupy it. This phenomenon is mainly influenced by the polarization properties of the ions. In particular, the electronegativity of bismuth and zinc atoms according to Allred–Rochow coincides and is equal to 1.67, and the electronegativity of magnesium is significantly less at 1.23 and is closer to the electronegativity of tantalum [34].

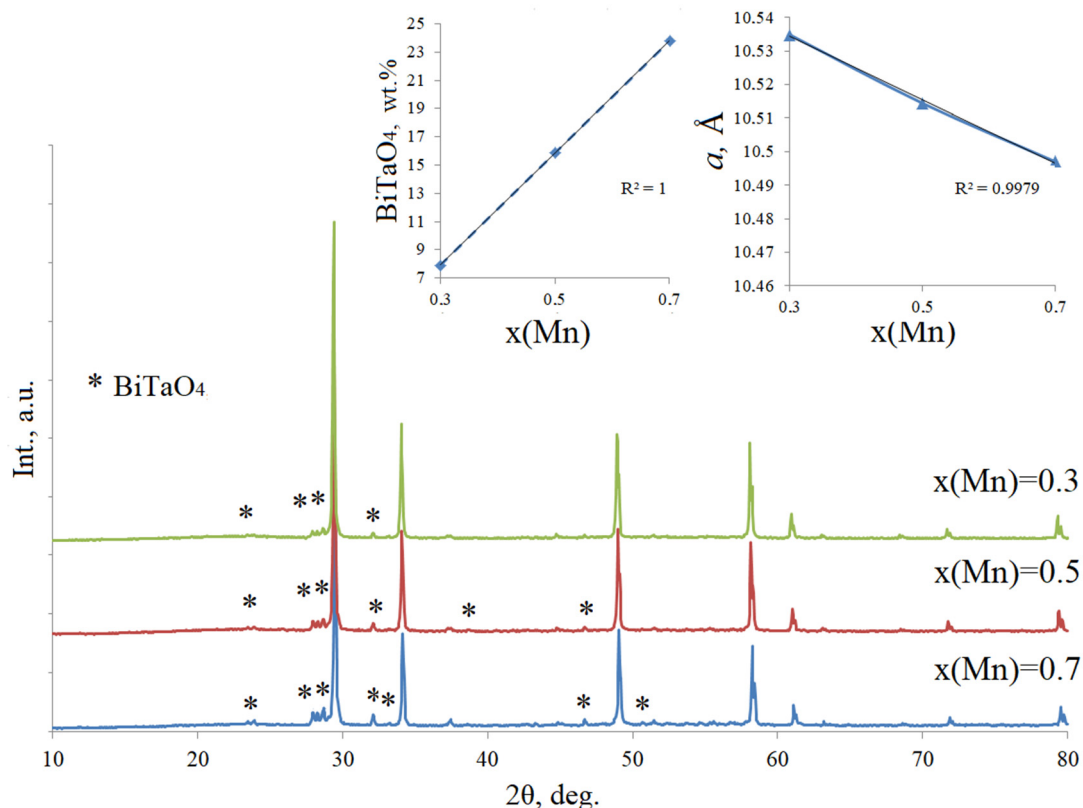


**Figure 2.** X-ray diffraction patterns of  $\text{Bi}_2\text{Mg}_x\text{Mn}_{1-x}\text{Ta}_2\text{O}_{9.5-\Delta}$  samples at different values of the  $x(\text{Mn})$  index. The inset shows the dependence of the amount of  $\text{BiTaO}_4$  and the unit cell parameter of pyrochlore on the  $x(\text{Mn})$  index.

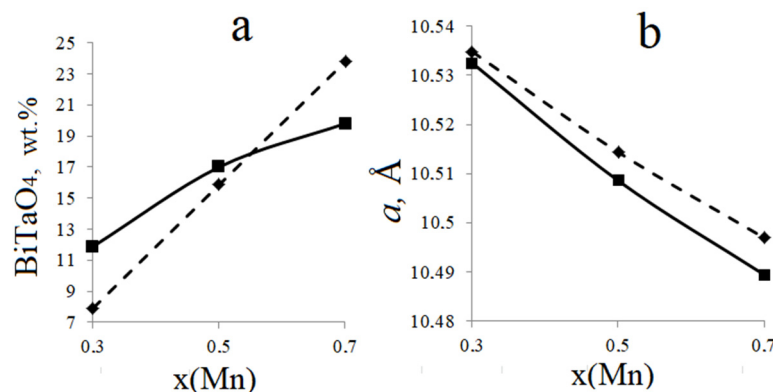


**Figure 3.** Comparison of the amount of BiTaO<sub>4</sub> impurity (a) and the unit cell parameter of the Bi<sub>2</sub>Mg<sub>x</sub>Mn<sub>1-x</sub>Ta<sub>2</sub>O<sub>9.5-Δ</sub> (dotted lines) and Bi<sub>2</sub>Zn<sub>x</sub>Mn<sub>1-x</sub>Ta<sub>2</sub>O<sub>9.5-Δ</sub> samples (solid lines) at different values of the x(Mn) index (b).

The lower amount of impurities in zinc preparations at  $x(\text{Mn}) > 0.5$  is explained by the lower content of Mn(II) ions compared to magnesium preparations (Figure 3). X-ray spectroscopy data shows that the amount of oxidized manganese(III) ions throughout the entire concentration range is greater in zinc preparations than in magnesium preparations. Earlier, we observed this interesting experimental fact while studying the magnetic behavior of solid solutions of heterovalent substitution Bi<sub>5</sub>Nb<sub>3-3x</sub>Mn<sub>3x</sub>O<sub>15-δ</sub> and Bi<sub>2</sub>BaNb<sub>2-2x</sub>Mn<sub>2x</sub>O<sub>9-δ</sub> [35,36]. It has been shown that with an increase in manganese dopant ions, the proportion of oxidized manganese ions increases in order to neutralize the effect of heterovalent substitution and reduce the number of oxygen vacancies that destabilize the crystal structure. In this case, the difference between magnesium and zinc preparations is based on the degree of distortion of the octahedral framework when replacing Ta(V) positions. Apparently, zinc ions, unlike magnesium ions, cause significant geometric distortions of the polyhedral environment due to a tendency towards tetrahedral coordination. These distortions affect the oxygen environment of manganese ions, resulting in an asymmetrical environment. In order to stabilize the oxygen framework, manganese ions pass into an oxidized state. It is interesting to note that in the competition to occupy bismuth positions, zinc ions are less effective than manganese(II) ions. This can be attributed to the difference in ionic radii between zinc and manganese(II) ( $R(\text{Zn(II)})_{\text{c.n-6}} = 0.74 \text{ \AA}$ ,  $R(\text{Mn(II)})_{\text{c.n-6}} = 0.83 \text{ \AA}$ ).

The unit cell parameter of pyrochlore in magnesium compositions Bi<sub>2</sub>Mg<sub>x</sub>Mn<sub>1-x</sub>Ta<sub>2</sub>O<sub>9.5-Δ</sub> is greater than in similar zinc compositions (Figure 3). This can occur due to two reasons. Firstly, BiTaO<sub>4</sub> impurities in zinc compositions are significantly higher than in magnesium compositions, but only for compositions with  $x(\text{Mn}) < 0.5$ . Secondly, in zinc compositions, the proportion of oxidized manganese (+3) ions is higher than in magnesium compositions. The unit cell parameter decreases when octahedrally coordinated and oxidized manganese ions are present, due to their radius being small compared to magnesium Mg(II) and Ta(V) ( $R(\text{Mn(IV)})_{\text{c.n-6}} = 0.53 \text{ \AA}$ ,  $R(\text{Mn(III)})_{\text{c.n-6}} = 0.645 \text{ \AA}$ ,  $R(\text{Mg(II)})_{\text{c.n-6}} = 0.72 \text{ \AA}$ ,  $R(\text{Ta(V)})_{\text{c.n-6}} = 0.64 \text{ \AA}$ ). NEXAFS studies show that zinc compositions have a higher proportion of oxidized manganese ions than magnesium compositions, with comparable amounts of impurities.

### 3.2. NEXAFS and XPS of the Bi<sub>2</sub>Mg(Zn)<sub>x</sub>Mn<sub>1-x</sub>Ta<sub>2</sub>O<sub>9.5-Δ</sub>

The electronic state of ions in Zn(Mg),Mn-codoped bismuth tantalate pyrochlores was studied using X-ray spectroscopy methods (NEXAFS and XPS). XPS spectra of Bi<sub>2</sub>MgTa<sub>2</sub>O<sub>9</sub> and Bi<sub>2</sub>Mg<sub>x</sub>Mn<sub>1-x</sub>Ta<sub>2</sub>O<sub>9.5-Δ</sub> ( $x = 0.5, 0.7$ ) precursor oxides are presented in Figure 4a–f.

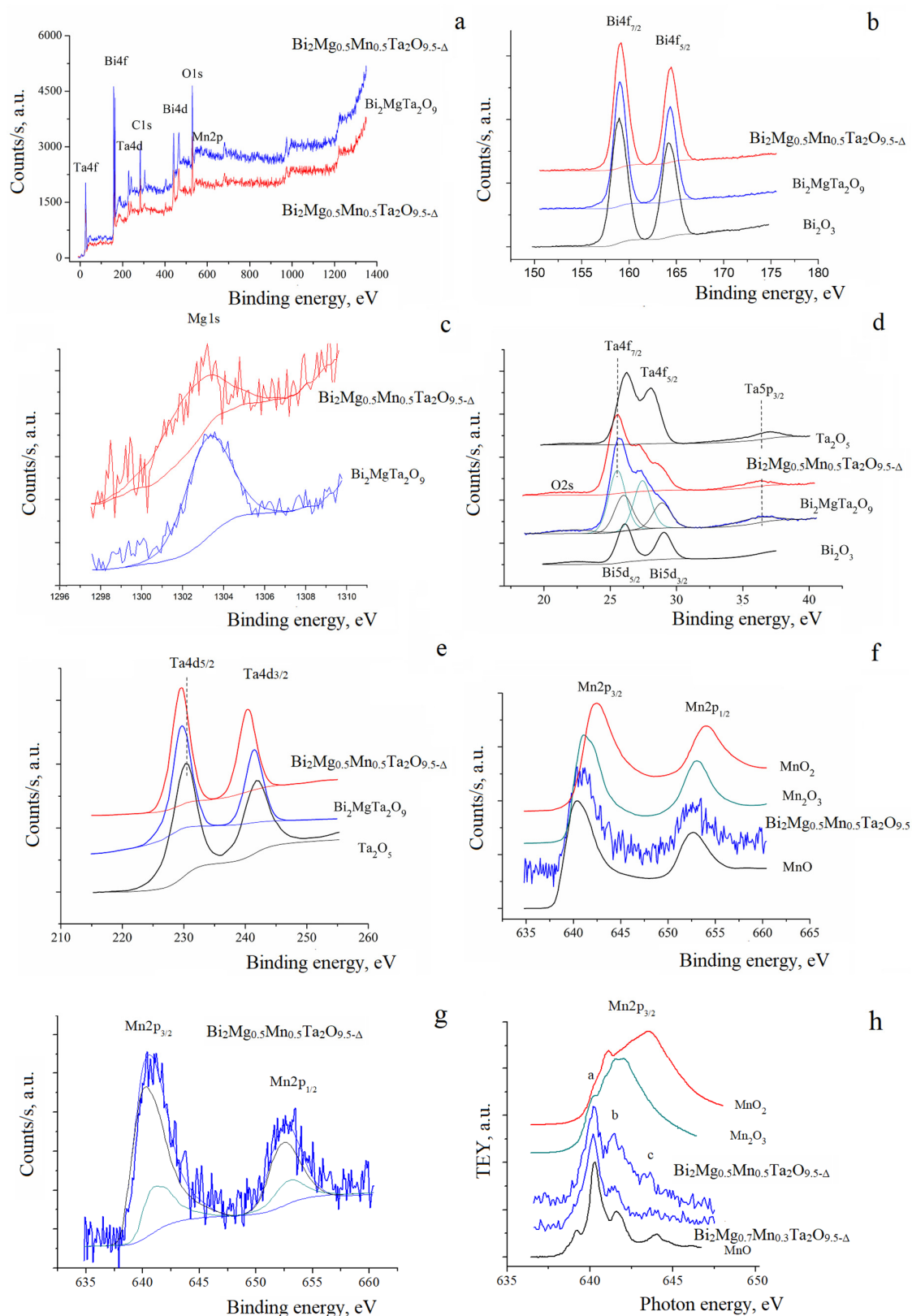


**Figure 4.** XPS spectra of  $\text{Bi}_2\text{Mg}_x\text{Mn}_{1-x}\text{Ta}_2\text{O}_{9.5-\Delta}$  and  $\text{Bi}_2\text{MgTa}_2\text{O}_9$  together with manganese and tantalum oxides: survey (a); Bi 4f (b); Mg 1s (c); Ta 4f, Ta 5p and Bi 5d (d); Ta 4d (e); and Mn 2p (f); XPS Mn 2p spectrum of  $\text{Bi}_2\text{Mg}_{0.5}\text{Mn}_{0.5}\text{Ta}_2\text{O}_9$  as a superposition of the spectra of Mn(II) and Mn(III) ions (g); NEXAFS Mn 2p spectra of  $\text{Bi}_2\text{Mg}_{0.5}\text{Mn}_{0.5}\text{Ta}_2\text{O}_9$  and  $\text{Bi}_2\text{Mg}_{0.7}\text{Mn}_{0.3}\text{Ta}_2\text{O}_{9.5-\Delta}$  and manganese oxides (h).

Figure 4a shows XPS spectra in a wide binding energies range (20–1400 eV) and in the region of the Bi4f-, Bi5d-, Ta4f-, Ta4d- and Mn2p-ionization thresholds of  $\text{Bi}_2\text{Mg}_{0.5}\text{Mn}_{0.5}\text{Ta}_2\text{O}_{9.5-\Delta}$  and  $\text{Bi}_2\text{MgTa}_2\text{O}_9$  (Figure 4a–f). The spectral dependences were decomposed into individual peaks by Gaussian–Lorentzian curves and the background lines were modeled by Shirley or smart approximation. The XPS survey spectrum exhibits a C1s peak indicating the presence of organic contaminants on the sample surface. Since the signal from surface contaminants contributes to the intensity of the O1s peak, the composition of the sample surface was characterized using metal ion spectra. The energy positions of the components in the measured XPS spectra of the samples are presented in Table 1. It should be noted that the doping with manganese and magnesium atoms has almost no effect on the spectral characteristics of bismuth and tantalum atoms (Figure 4b,d,e). The XPS spectra of the oxides  $\text{Bi}_2\text{O}_3$  and  $\text{Ta}_2\text{O}_5$  (Figures 4 and 5) were obtained by our research group. The comparative analysis of the XPS Bi4f spectra of the investigated sample and  $\text{Bi}_2\text{O}_3$  oxide (Figure 4b,d) highlights that the energy position and width of the peaks in the sample spectrum correlate with the corresponding spectra of  $\text{Bi}_2\text{O}_3$  oxide. It is notable that the Bi5d<sub>3/2</sub>, Bi5d<sub>5/2</sub>, Bi4f<sub>7/2</sub>, and Bi4f<sub>5/2</sub> absorption bands of the  $\text{Bi}_2\text{Mg}_{0.5}\text{Mn}_{0.5}\text{Ta}_2\text{O}_{9.5-\Delta}$  sample are slightly shifted to a lower energy region compared to the  $\text{Bi}_2\text{MgTa}_2\text{O}_9$  sample, from 164.12 eV to 164.35 eV (for Bi4f<sub>5/2</sub> band), respectively. This fact indicates a decrease in the effective charge of bismuth ions in the samples. Apparently, the shift of the peaks is associated with the placement of a certain fraction of divalent manganese(II) ions in the bismuth position demonstrated by X-ray phase analysis. The energy positions of the peaks in the XPS Mg1s spectra shown in Figure 4c are typical for the divalent magnesium atom [37]. The analysis of the peak shape in the spectrum of tantalum atoms (Figure 4d,e) indicates that all tantalum atoms are in the same charge state. However, the energy position of the peaks shows a characteristic shift towards lower energies compared to the binding energy in pentavalent tantalum oxide  $\text{Ta}_2\text{O}_5$ . This shift towards lower energies indicates a decrease in the effective positive charge. Specifically, Ta4f and Ta5p spectra exhibit an energy shift of  $\Delta E = 0.7$  eV, while the Ta4d spectra exhibit an energy shift of 1 eV. This suggests that tantalum atoms have the same effective charge  $+(5-\delta)$  as observed in similar spectra of tantalum in bismuth tantalates doped with Cr, Fe, Co, Ni, Cu atoms [21,22,24]. The shift of the Ta4f and Ta5p spectra for  $\text{Bi}_2\text{Mg}_{0.5}\text{Mn}_{0.5}\text{Ta}_2\text{O}_{9.5-\Delta}$  and  $\text{Bi}_2\text{MgTa}_2\text{O}_9$  may also be associated with the presence of a certain fraction of heterovalent manganese and magnesium ions in the tantalum(V) position.

**Table 1.** Energy positions of the components of XPS spectra depending on the chemical composition of the compounds.

Peak	Chemical Composition of Compounds			
	$\text{Bi}_2\text{Mg}_{0.5}\text{Mn}_{0.5}\text{Ta}_2\text{O}_{9.5-\Delta}$	$\text{Bi}_2\text{MgTa}_2\text{O}_9$	$\text{Bi}_2\text{Zn}_{0.3}\text{Mn}_{0.7}\text{Ta}_2\text{O}_{9.5-\Delta}$	$\text{Bi}_2\text{Zn}_{0.7}\text{Mn}_{0.3}\text{Ta}_2\text{O}_{9.5-\Delta}$
	Energy (eV)			
Bi4f <sub>7/2</sub>	158.80	159.03	158.81	158.79
Bi4f <sub>5/2</sub>	164.12	164.35	164.13	164.10
Bi5d <sub>5/2</sub>	25.82	26.11	25.81	25.87
Bi5d <sub>3/2</sub>	28.72	29.08	28.71	28.78
Ta4f <sub>7/2</sub>	25.31	25.66	25.35	25.41
Ta4f <sub>5/2</sub>	27.21	27.56	27.25	27.31
Mg1s	1302.49	1303.19		
Mn2p <sub>3/2</sub>	640.83		640.98	640.71
Mn2p <sub>1/2</sub>	652.39		652.75	652.51
Zn2p <sub>3/2</sub>			1021.07	1020.98
Zn2p <sub>1/2</sub>			1044.10	1043.99

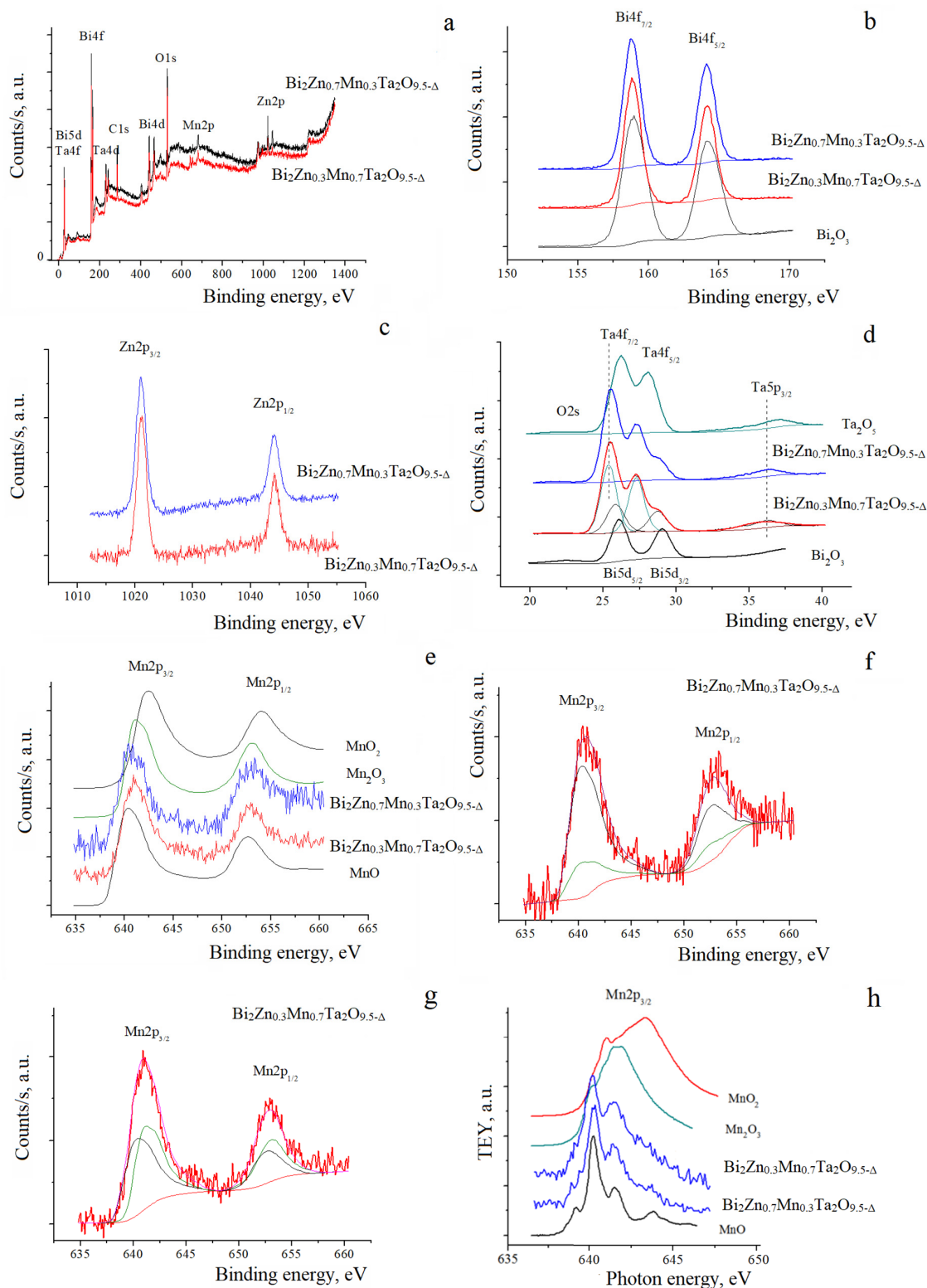


**Figure 5.** Survey XPS spectra of  $\text{Bi}_2\text{Zn}_x\text{Mn}_{1-x}\text{Ta}_2\text{O}_{9.5-\Delta}$  ( $x = 0.3$  and  $0.7$ ) (a); XPS Bi4f<sub>7/2</sub> and Bi4f<sub>5/2</sub> spectra of bismuth (b); XPS Zn2p spectra (c); XPS spectra of tantalum and bismuth in  $\text{Bi}_2\text{Zn}_x\text{Mn}_{1-x}\text{Ta}_2\text{O}_{9.5-\Delta}$  in  $\text{Bi}_2\text{O}_3$  and  $\text{Ta}_2\text{O}_5$  oxides (d); XPS Mn2p spectra in  $\text{Bi}_2\text{Zn}_x\text{Mn}_{1-x}\text{Ta}_2\text{O}_{9.5-\Delta}$  in the oxides MnO, Mn<sub>2</sub>O<sub>3</sub> and MnO<sub>2</sub> (e); decomposition of XPS Mn2p spectra in  $\text{Bi}_2\text{Zn}_x\text{Mn}_{1-x}\text{Ta}_2\text{O}_{9.5-\Delta}$  into Mn(II) and Mn(III)-green line (f,g); NEXAFS Mn2p spectra in  $\text{Bi}_2\text{Zn}_x\text{Mn}_{1-x}\text{Ta}_2\text{O}_{9.5-\Delta}$  ( $x = 0.3$  and  $0.7$ ) and manganese oxides (h).

Let us move on to consider the Mn2p spectra presented in Figure 4f. The comparative analysis of the composite spectra with the spectra of the oxides MnO [38], Mn<sub>2</sub>O<sub>3</sub> [39] and MnO<sub>2</sub> [40] from the literature data shows that the peak energy positions of the spectrum of Bi<sub>2</sub>Mg<sub>0.5</sub>Mn<sub>0.5</sub>Ta<sub>2</sub>O<sub>9.5-Δ</sub> correlates well with the spectrum of MnO, while the spectra of Mn<sub>2</sub>O<sub>3</sub> and MnO<sub>2</sub> are shifted towards higher energies. This suggests that manganese ions predominantly have an oxidation state of (2+). Figure 4f shows the incomplete energy coincidence of the components of the spectrum of manganese in MnO and Bi<sub>2</sub>Mg<sub>0.5</sub>Mn<sub>0.5</sub>Ta<sub>2</sub>O<sub>9.5-Δ</sub>, indicating the presence of oxidized manganese ions (3+, 4+). The degree of oxidation of manganese in solid solutions was clarified by NEXAFS studies. Figure 4h shows the NEXAFS Mn2p spectra of Bi<sub>2</sub>Mg<sub>0.5</sub>Mn<sub>0.5</sub>Ta<sub>2</sub>O<sub>9.5-Δ</sub> and Bi<sub>2</sub>Mg<sub>0.3</sub>Mn<sub>0.7</sub>Ta<sub>2</sub>O<sub>9.5-Δ</sub> and manganese oxides. The correlation between the spectra shape and energy position of the main peaks (a-c) in the NEXAFS Mn2p spectra of all samples and in oxides indicates that the manganese atoms primarily have a charge state of +2. It should be noted that band c, which can be identified as a separate peak in the spectrum of MnO, is visible in the spectra of the samples as a shoulder. In addition, the relative intensity of the b bands also increases compared to the MnO spectrum. Shoulder c coincides in energy position with a broad band in the spectrum of MnO<sub>2</sub>, and bands a and b correlate well with the corresponding features in the spectra of Mn<sub>2</sub>O<sub>3</sub>, but with different intensities. This suggests that the manganese atoms in the composites are both in the +2-charge state and partially in the +3/+4 state. To clarify this conclusion, we decomposed the XPS Mn2p spectra of the Bi<sub>2</sub>Mg<sub>0.5</sub>Mn<sub>0.5</sub>Ta<sub>2</sub>O<sub>9.5-Δ</sub> sample into individual components (Figure 4g) using the spectra of the oxides presented in Figure 4f. The decomposition occurred in multiple stages: (1) subtraction of the background lines obtained using the Shirley approximation, (2) the “background-free” XPS spectra were normalized by equal areas (in this case, one was taken), (3) a model spectrum was constructed as the sum of the XPS spectra of MnO, Mn<sub>2</sub>O<sub>3</sub> and MnO<sub>2</sub> with the corresponding coefficients  $\alpha$ ,  $\beta$  and  $\gamma$  ( $\alpha + \beta + \gamma = 1$ ). The value of coefficients was selected in order to achieve the best possible agreement with the composite spectrum. The Fisher F-criterion was used to determine optimal agreement between intensities of the XPS spectra of the composite and the model spectrum. The results of optimal modeling are presented in Figure 4h, with  $\alpha = 0.77$ ,  $\beta = 0.23$  and  $\gamma = 0$  (Fisher’s F test is 0.9998). The obtained data suggest that the Bi<sub>2</sub>Mg<sub>0.5</sub>Mn<sub>0.5</sub>Ta<sub>2</sub>O<sub>9.5-Δ</sub> composite has two nonequivalent states of manganese atoms: about 77% are in the +2-charge state, and the remaining 23% are in +3 state. This fact allows us to conclude that the intense b band presented in the NEXAFS spectra (Figure 4h) indicates the presence of Mn<sup>3+</sup> ions in the composite. Moreover, with increasing manganese content in Bi<sub>2</sub>Mg<sub>x</sub>Mn<sub>1-x</sub>Ta<sub>2</sub>O<sub>9.5-Δ</sub>, the intensity of this peak also increases, indicating an increase in Mn<sup>3+</sup> ion content. Figure 5a–f shows the XPS spectra of Bi<sub>2</sub>Zn<sub>x</sub>Mn<sub>1-x</sub>Ta<sub>2</sub>O<sub>9.5-Δ</sub> ( $x = 0.3$  and  $0.7$ ) and the initial metal (Bi and Mn) oxides used in the sample synthesis. Table 1 summarizes the energy positions of the separated peaks in the measured spectra. As in the case of composition with Mn, Mg, doping with manganese atoms does not change the spectral characteristics of bismuth, tantalum and zinc atoms (Figure 5). Comparing the XPS Bi4f spectra of the sample under study and Bi<sub>2</sub>O<sub>3</sub> oxide (Figure 5b) highlights the energy position and width of the peaks in the spectra of the samples almost completely coincides and correlates well with the corresponding spectra of the oxide. In the case of Bi<sub>2</sub>Zn<sub>x</sub>Mn<sub>1-x</sub>Ta<sub>2</sub>O<sub>9.5-Δ</sub> samples, the position of the Bi4f7/2 and Bi4f5/2 bands correlates with the magnesium compositions. The sample spectrum shows a slight shift of the Bi4f7/2 and Bi4f5/2 absorption bands relative to the Bi<sub>2</sub>O<sub>3</sub> spectrum, both relative to each other and to the lower energy region in general. For example, the Bi4f5/2 band shifts from 164.10 eV ( $x = 0.7$ ) to 164.13 eV ( $x = 0.3$ ), indicating a decrease in the effective charge of bismuth ions with increasing x(Zn). This shift is associated with the placement of a certain fraction of divalent ions in the bismuth position. The observed concentration dependence also suggests the possible distribution of zinc ions in the bismuth position compared to manganese ions at large values of x(Zn). The energy positions of the peaks in the XPS Zn2p spectra shown in Figure 5c are characteristic of the divalent zinc ion [41]. When analyzing the spectra of tantalum ions (Figure 5d), it

is important to note that the peaks are not split or distorted. This clearly indicates that all tantalum atoms are in the same charge state. However, the energy position of the peaks has a characteristic shift towards lower energies compared to the binding energy in pentavalent tantalum oxide  $\text{Ta}_2\text{O}_5$  [42,43]. The shift towards lower energies is characteristic of a decrease in the effective positive charge; in particular, for the presented Ta4f and Ta5p spectra, the energy shift is  $\Delta E = 0.65$  eV, which suggests that tantalum ions have the same effective charge  $+(5-\delta)$ . Figure 5e shows the XPS Mn2p spectra of  $\text{Bi}_2\text{Zn}_x\text{Mn}_{1-x}\text{Ta}_2\text{O}_{9.5-\Delta}$  ( $x = 0.3$  and  $0.7$ ) samples and manganese oxides presented in a comparison of the composite spectra, with different manganese oxides spectra showing a strong correlation in the energy position of the peaks in both composite and MnO spectra. This led to the conclusion that manganese ions predominantly have an oxidation state of (2+). Figure 5e shows that there is no complete energy coincidence between the components of the spectrum of manganese in the composites and MnO, indicating the presence of oxidized manganese ions (3+, 4+). To clarify this conclusion, we attempted to decompose the XPS Mn2p spectra of the  $\text{Bi}_2\text{Zn}_{0.3}\text{Mn}_{0.7}\text{Ta}_2\text{O}_{9.5-\Delta}$  and  $\text{Bi}_2\text{Zn}_{0.7}\text{Mn}_{0.3}\text{Ta}_2\text{O}_{9.5-\Delta}$  samples into individual components according to the method described above, using the spectra of the oxides presented in Figure 5e. The results of optimal modeling for the  $\text{Bi}_2\text{Zn}_{0.7}\text{Mn}_{0.3}\text{Ta}_2\text{O}_{9.5-\Delta}$  sample ( $\alpha = 0.79$ ,  $\beta = 0.21$  and  $\gamma = 0$ ) and the  $\text{Bi}_2\text{Zn}_{0.3}\text{Mn}_{0.7}\text{Ta}_2\text{O}_{9.5-\Delta}$  sample ( $\alpha = 0.48$ ,  $\beta = 0.52$  and  $\gamma = 0$ ) are presented in Figure 5f and in Figure 5e, respectively. The obtained data indicate that the composites contain two nonequivalent states of manganese atoms: +2 and +3. Moreover, it was found that with increasing manganese content, the proportion of states with +3 increases from 0.21 to 0.52 in the total manganese content. The NEXAFS studies clarified the oxidation degree of manganese in solid solutions. Figure 5h shows the NEXAFS Mn2p spectra of  $\text{Bi}_2\text{Zn}_{0.3}\text{Mn}_{0.7}\text{Ta}_2\text{O}_{9.5-\Delta}$  and  $\text{Bi}_2\text{Zn}_{0.7}\text{Mn}_{0.3}\text{Ta}_2\text{O}_{9.5-\Delta}$  and manganese oxides. The comparison of the samples and oxides spectra draws our attention to the shape of the spectra; the energy position of the main peaks of the samples (640.3 and 641.5) correlate with the spectra of MnO. This suggests that the manganese atoms in the studied samples are primarily in +2 charge state. Moreover, some spectra features indicate the presence of oxidized manganese (III, IV) ions in the samples. This is indicated by the absence of clear absorption lines at 644 and 639 eV, which appear in the spectrum of MnO. Additionally, the ratio of the intensities of the lines at 640.3 and 641.5 eV observed in the spectra of the samples is lower than for the lines in the MnO spectrum.

The lines in the Mn2p spectra of the samples appear broad and diffuse compared to MnO, which could be due to the superposition of the spectra of manganese ions in different oxidation states. In addition, the ratio of line intensities at 640.3 and 641.5 eV is not constant for the  $\text{Bi}_2\text{Zn}_x\text{Mn}_{1-x}\text{Ta}_2\text{O}_{9.5-\Delta}$  samples ( $x = 0.3$  and  $0.7$ ). The line intensities ratio decreases with the manganese content  $x(\text{Mn})$  increases, which indicates a variable ionic composition of manganese in the samples and a higher concentration of oxidized manganese ions in samples with the highest manganese content, which is consistent with XPS data. Thus, it can be concluded that in the XPS spectra of both series bismuth and tantalum samples there is an energy shift of the absorption bands towards lower energy values, depending on the dopant content. This shift is typical for bismuth and tantalum ions with an effective charge of  $(+3-\delta)$  and  $(+5-\delta)$ , respectively, due to the distribution of some of the transition elements ions in the position of bismuth and tantalum. According to NEXAFS and XPS spectroscopy data, the manganese ions in the samples have predominantly +2 and +3 oxidation states. According to X-ray spectroscopy data, zinc-containing preparations exhibit a higher proportion of oxidized manganese(III) ions compared to magnesium compounds. In both series of samples, the proportion of oxidized manganese ions increases with increasing manganese content.

#### 4. Conclusions

The  $\text{Bi}_2\text{Mg}(\text{Zn})_x\text{Mn}_{1-x}\text{Ta}_2\text{O}_{9.5-\Delta}$  composites were synthesized by the solid-phase method. X-ray diffraction analysis indicates that the composites contain a  $\text{BiTaO}_4$  impurity which is directly proportional to the amount of manganese content. The unit cell parameter

of the pyrochlore phase increases with increasing zinc or magnesium content in the samples. The XPS spectra of both samples' series show an energy shift towards the lower energy region of the bismuth absorption bands (Bi4f7/2 and Bi4f5/2), which is associated with the presence of some transition element ions in the bismuth position. According to NEXAFS and XPS data, it was established that the charge states of bismuth, zinc, and magnesium ions are Bi(+3- $\delta$ ), Zn(+2), Mg(+2). The XPS Ta4f spectrum of Bi<sub>2</sub>Mg(Zn)<sub>x</sub>Mn<sub>1-x</sub>Ta<sub>2</sub>O<sub>9.5- $\Delta$</sub>  demonstrates a lower energy shift of the absorption band by  $\Delta E = 0.7$  and 0.65 eV compared to the Ta<sub>2</sub>O<sub>5</sub> spectrum. This shift allows us to estimate the oxidation state of tantalum ions as Ta(+5- $\delta$ ). It has been shown that doping pyrochlores with zinc or magnesium ions leads to the oxidation of some manganese ions to Mn(III). This effect is particularly significant in zinc-containing samples.

**Author Contributions:** Conceptualization, N.A.Z.; Funding acquisition, S.V.N., O.V.P. and V.N.S. Investigation, B.A.M., A.V.K., A.M.L., N.A.Z. and S.V.N.; Resources, A.V.K., A.M.L., O.V.P., V.N.S. and B.A.M.; Validation, N.A.Z.; Visualization, S.V.N. and N.A.Z.; Writing—original draft, N.A.Z. All authors have read and agreed to the published version of the manuscript.

**Funding:** This research (in part of NEXAFS) was funded by the Ministry of Science and Higher Education of Russia grant number 075-15-2021-1351.

**Data Availability Statement:** The data presented in this study are available in article.

**Acknowledgments:** The XPS studies were performed on the equipment of the Resource Center "Physical methods of surface investigation" of the Scientific Park of St. Petersburg University. The NEXAFS studies were performed on the synchrotron radiation from station "NanoPES" storage ring (National Research Center "Kurchatov Institute").

**Conflicts of Interest:** The authors declare no conflict of interest.

## References

1. Vanderah, T.A.; Levin, I.; Lufaso, M.W. An Unexpected Crystal-Chemical Principle for the Pyrochlore Structure. *Eur. J. Inorg. Chem.* **2005**, *14*, 2895–2901. [[CrossRef](#)]
2. Hiroi, Z.; Yamaura, J.-I.; Yonezawa, S.; Harima, H. Chemical trends of superconducting properties in pyrochlore oxides. *Phys. C Supercond. Appl.* **2007**, *460–462*, 20–27. [[CrossRef](#)]
3. Du, H.; Yao, X. Structural trends and dielectric properties of Bi-based pyrochlores. *J. Mater. Sci. Mater. Electron.* **2004**, *15*, 613–616.
4. Bongers, P.F.; Van Meurs, E.R. Ferromagnetism in Compounds with Pyrochlore Structure. *J. Appl. Phys.* **1967**, *38*, 944–945. [[CrossRef](#)]
5. Greedan, J.E. Frustrated rare earth magnetism: Spin glasses, spin liquids and spin ices in pyrochlore oxides. *J. Alloys Compd.* **2006**, *408–412*, 444–455. [[CrossRef](#)]
6. Egorysheva, A.V.; Ellert, O.G.; Popova, E.F.; Kiryankin, D.I.; Maksimov, Y.V. Weak ferromagnetism in a diamagnetically diluted sublattice of Fe<sup>3+</sup> ions in solid solutions Y<sub>2-x</sub>Fe<sub>1+x</sub>TaO<sub>7</sub> (x = 0–0.2) with pyrochlore-like structure. *Mendeleev Commun.* **2023**, *33*, 519–521. [[CrossRef](#)]
7. Giampaoli, G.; Siritanon, T.; Day, B.; Li, J.; Subramanian, M.A. Temperature in-dependent low loss dielectrics based on quaternary pyrochlore oxides. *Prog. Solid State Chem.* **2018**, *50*, 16–23. [[CrossRef](#)]
8. Murugesan, S.; Huda, M.N.; Yan, Y.; Al-Jassim, M.M.; Subramanian, V. Band-Engineered Bismuth Titanate Pyrochlores for Visible Light Photocatalysis. *J. Phys. Chem. C* **2010**, *114*, 10598–10605. [[CrossRef](#)]
9. Khaw, C.C.; Tan, K.B.; Lee, C.K. High temperature dielectric properties of cubic bismuth zinc tantalate. *Ceram. Intern.* **2009**, *35*, 1473–1480. [[CrossRef](#)]
10. Subramanian, M.A.; Aravamudan, G.; Subba Rao, G.V. Oxide pyrochlores—A review. *Prog. Solid State Chem.* **1983**, *15*, 55–143. [[CrossRef](#)]
11. McCauley, R.A. Structural Characteristics of Pyrochlore Formation. *J. Appl. Phys.* **1980**, *51*, 290–294. [[CrossRef](#)]
12. Nguyen, H.B.; Noren, L.; Liu, Y.; Withers, R.L.; Wei, X.R.; Elcombe, M.M. The disordered structures and low temperature dielectric relaxation properties of two misplaced-displacive cubic pyrochlores found in the Bi<sub>2</sub>O<sub>3</sub>-MO-Nb<sub>2</sub>O<sub>5</sub> (M=Mg,Ni) systems. *J. Sol. St. Chem.* **2007**, *180*, 2558–2565. [[CrossRef](#)]
13. Levin, I.; Amos, T.G.; Nino, J.C.; Vanderah, T.A.; Randall, C.A.; Lanagan, M.T. Structural Study of an Unusual Cubic Pyrochlore Bi<sub>1.5</sub>Zn<sub>0.92</sub>Nb<sub>1.5</sub>O<sub>6.92</sub>. *J. Solid State Chem.* **2002**, *168*, 69–75. [[CrossRef](#)]
14. Lufaso, M.W.; Vanderah, T.A.; Pazos, I.M.; Levin, I.; Roth, R.S.; Nino, J.C.; Provenzano, V.; Schenck, P.K. Phase formation, crystal chemistry, and properties in the system Bi<sub>2</sub>O<sub>3</sub>-Fe<sub>2</sub>O<sub>3</sub>-Nb<sub>2</sub>O<sub>5</sub>. *J. Solid State Chem.* **2006**, *179*, 3900–3910. [[CrossRef](#)]
15. Vanderah, T.A.; Lufaso, M.W.; Adler, A.U.; Levin, I.; Nino, J.C.; Provenzano, V.; Schenck, P.K. Subsidiary phase equilibria and properties in the system Bi<sub>2</sub>O<sub>3</sub>:Mn<sub>2</sub>O<sub>3</sub>±x:Nb<sub>2</sub>O<sub>5</sub>. *J. Solid State Chem.* **2006**, *179*, 3467–3477. [[CrossRef](#)]

16. Vanderah, T.A.; Siegrist, T.; Lufaso, M.W.; Yeager, M.C.; Roth, R.S.; Nino, J.C.; Yates, S. Phase Formation and Properties in the System  $\text{Bi}_2\text{O}_3\cdot 2\text{CoO}_{1+x}\cdot \text{Nb}_2\text{O}_5$ . *Eur. J. Inorgan. Chem.* **2006**, *2006*, 4908–4914. [[CrossRef](#)]
17. Kamba, S.; Porokhonsky, V.; Pashkin, A.; Bovtun, V.; Petzelt, J.; Nino, J.C.; Trolier-McKinstry, S.; Lanagan, M.T.; Randall, C.A. Anomalous broad dielectric relaxation in  $\text{Bi}_{1.5}\text{Zn}_{1.0}\text{Nb}_{1.5}\text{O}_7$  pyrochlore. *Phys. Rev. B* **2002**, *66*, 054106. [[CrossRef](#)]
18. Ismunandar; Kamiyama, T.; Oikawa, K.; Hoshikawa, A.; Kennedy, B.J.; Kubota, Y.; Kato, K. Static bismuth disorder in  $\text{Bi}_{2-x}(\text{CrTa})\text{O}_{7-y}$ . *Mater. Res. Bull.* **2004**, *39*, 553–560. [[CrossRef](#)]
19. Egorysheva, A.V.; Ellert, O.G.; Popova, E.F.; Kirdyankin, D.I.; Khramov, E.V.; Maksimov, Y.V. Phase Equilibria in the  $\text{Sm}_2\text{O}_3\text{--Fe}_2\text{O}_3\text{--Ta}_2\text{O}_5$  System: Structural Transitions and Magnetic Properties of the Solid Solution  $\text{Sm}_{2-x}\text{Fe}_1 + x\text{TaO}_7$ . *Russ. J. Inorg. Chem.* **2022**, *67*, 1695–1705. [[CrossRef](#)]
20. Zhuk, N.A.; Krzhizhanovskaya, M.G.; Sekushin, N.A.; Sivkov, D.V.; Abdurakhmanov, I.E. Crystal structure, dielectric and thermal properties of cobalt doped bismuth tantalate pyrochlore. *J. Mater. Res. Technol.* **2023**, *22*, 1791–1799. [[CrossRef](#)]
21. Zhuk, N.A.; Krzhizhanovskaya, M.G.; Sekushin, N.A.; Kharton, V.V.; Koroleva, A.V.; Nekipelov, S.V.; Sivkov, D.V.; Sivkov, V.N.; Makeev, B.A.; Lebedev, A.M.; et al. Novel Ni-Doped Bismuth–Magnesium Tantalate Pyrochlores: Structural and Electrical Properties, Thermal Expansion, X-ray Photoelectron Spectroscopy, and Near-Edge X-ray Absorption Fine Structure Spectra. *ACS Omega* **2021**, *6*, 23262–23273. [[CrossRef](#)]
22. Zhuk, N.A.; Krzhizhanovskaya, M.G.; Koroleva, A.V.; Sekushin, N.A.; Nekipelov, S.V.; Kharton, V.V.; Sennikova, Y.D. Cu, Mg Codoped Bismuth Tantalate Pyrochlores: Crystal Structure, XPS Spectra, Thermal Expansion, and Electrical Properties. *Inorg. Chem.* **2022**, *61*, 4270–4282. [[CrossRef](#)]
23. Chon, M.P.; Tan, K.B.; Khaw, C.C.; Zainal, Z.; Taufiq-Yap, Y.H.; Chen, S.K.; Tan, P.Y. Subsolidus phase equilibria and electrical properties of pyrochlores in the  $\text{Bi}_2\text{O}_3\text{--CuO--Ta}_2\text{O}_5$  ternary system. *J. Alloys Compd.* **2016**, *675*, 116–127. [[CrossRef](#)]
24. Egorysheva, A.V.; Popova, E.F.; Tyurin, A.V.; Khoroshilov, A.V. Synthesis and Thermodynamic Properties of the  $\text{Ln}_2\text{CrTaO}_7$  ( $\text{Ln} = \text{Sm, Gd, Y}$ ) Pyrochlores. *Russ. J. Inorg. Chem.* **2021**, *66*, 1649–1659. [[CrossRef](#)]
25. Youn, H.-J.; Sogabe, T.; Randall, C.A.; Shrout, T.R.; Lanagan, M.T. Phase Relations and Dielectric Properties in the  $\text{Bi}_2\text{O}_3\text{--ZnO--Ta}_2\text{O}_5$  System. *J. Am. Ceram. Soc.* **2001**, *84*, 2557–2562. [[CrossRef](#)]
26. Khaw, C.C.; Tan, K.B.; Lee, C.K.; West, A.R. Phase equilibria and electrical properties of pyrochlore and zirconolite phases in the  $\text{Bi}_2\text{O}_3\text{--ZnO--Ta}_2\text{O}_5$  system. *J. Eur. Ceram. Soc.* **2012**, *32*, 671–680. [[CrossRef](#)]
27. Jusoh, F.A.; Tan, K.B.; Zainal, Z.; Chen, S.K.; Khaw, C.C.; Lee, O.J. Novel pyrochlores in the  $\text{Bi}_2\text{O}_3\text{--Fe}_2\text{O}_3\text{--Ta}_2\text{O}_5$  (BFT) ternary system: Synthesis, structural and electrical properties. *J. Mater. Res. Technol.* **2020**, *9*, 11022–11034. [[CrossRef](#)]
28. Tan, P.Y.; Tan, K.B.; Khaw, C.C.; Zainal, Z.; Chen, S.K.; Chon, M.P. Phase equilibria and dielectric properties of  $\text{Bi}_{3+(5/2)x}\text{Mg}_{2-x}\text{Nb}_{3-(3/2)x}\text{O}_{14-x}$  cubic pyrochlores. *Ceram. Intern.* **2014**, *40*, 4237–4246. [[CrossRef](#)]
29. Tan, P.Y.; Tan, K.B.; Khaw, C.; Zainal, Z.; Chen, S.K.; Chon, M.P. Structural and electrical properties of bismuth magnesium tantalate pyrochlores. *Ceram. Intern.* **2012**, *38*, 5401–5409. [[CrossRef](#)]
30. Lebedev, A.M.; Menshikov, K.A.; Nazin, V.G.; Stankevich, V.G.; Tsetlin, M.B.; Chumakov, R.G. NanoPES Photoelectron Beamline of the Kurchatov Synchrotron Radiation Source. *J. Surface Investig. X-ray Synchrotron Neutron Tech.* **2021**, *15*, 1039–1044. [[CrossRef](#)]
31. Muktha, B.; Darriet, J.; Madras, G.; Guru Row, T.N. Crystal structures and photocatalysis of the triclinic polymorphs of  $\text{BiNbO}_4$  and  $\text{BiTaO}_4$ . *J. Solid State Chem.* **2006**, *179*, 3919–3925. [[CrossRef](#)]
32. Shannon, R.D. Revised effective ionic radii and systematic studies of interatomic distances in halides and chalcogenides. *Acta Crystallogr. A* **1976**, *32*, 751–767. [[CrossRef](#)]
33. Rylchenko, E.P.; Makeev, B.A.; Sivkov, D.V.; Korolev, R.I.; Zhuk, N.A. Features of phase formation of pyrochlore-type  $\text{Bi}_2\text{Cr}_{1/6}\text{Mn}_{1/6}\text{Fe}_{1/6}\text{Co}_{1/6}\text{Ni}_{1/6}\text{Cu}_{1/6}\text{Ta}_2\text{O}_{9+\Delta}$ . *Lett. Mater.* **2022**, *12*, 486–492. [[CrossRef](#)]
34. Allred, A.L.; Rochow, E.G. A scale of electronegativity based on electrostatic force. *J. Inorg. Nucl. Chem.* **1958**, *5*, 264–268. [[CrossRef](#)]
35. Chezhina, N.V.; Korolev, D.A.; Fedorova, A.V.; Zhuk, N.A.; Lutoev, V.P.; Makeev, B.A. Structure, magnetic, and electrical properties of bismuth niobates doped with d-elements: XVIII. Magnetic susceptibility and ESR spectra of  $\text{Bi}_2\text{BaNb}_{2-2x}\text{Mn}_{2x}\text{O}_{9-\delta}$  solid solutions with layered perovskite-like structure. *Russ. J. Gen. Chem.* **2017**, *87*, 2525–2532. [[CrossRef](#)]
36. Chezhina, N.V.; Korolev, D.A.; Fedorova, A.V.; Zhuk, N.A.; Shevchuk, S.S.; Nizovtsev, A.N. Structure, magnetic, and electrical properties of bismuth niobates doped with d-elements: XVII. Magnetic properties of  $\text{Bi}_5\text{Nb}_{3-3x}\text{Mn}_{3x}\text{O}_{15-\delta}$  solid solutions. *Russ. J. Gen. Chem.* **2017**, *87*, 2251–2257. [[CrossRef](#)]
37. Khairallah, F.; Glisenti, A. XPS Study of MgO Nanopowders Obtained by Different Preparation Procedures. *Surf. Sci. Spectra* **2006**, *13*, 58–71. [[CrossRef](#)]
38. Grissa, R.; Martinez, H.; Cotte, S.; Galipaud, J.; Pecquenard, B.; Cras, F.L. Thorough XPS analyses on overlithiated manganese spinel cycled around the 3V plateau. *Appl. Surf. Sci.* **2017**, *411*, 449–456. [[CrossRef](#)]
39. Stranick, M.A.  $\text{Mn}_2\text{O}_3$  by XPS. *Surf. Sci. Spectra* **1999**, *6*, 39–46. [[CrossRef](#)]
40. Gri, F.; Bigiani, L.; Gasparotto, A.; Maccato, C.; Barreca, D. XPS investigation of F-doped  $\text{MnO}_2$  nanosystems fabricated by plasma assisted-CVD. *Surf. Sci. Spectra* **2018**, *25*, 024004. [[CrossRef](#)]
41. Biesinger, M.C.; Lau, L.W.M.; Gerson, A.R.; Smart, R.S.C. Resolving surface chemical states in XPS analysis of first row transition metals, oxides and hydroxides: Sc, Ti, V, Cu and Zn. *Appl. Surf. Sci.* **2010**, *257*, 887–898. [[CrossRef](#)]

42. Sarma, D.D.; Rao, C.N.R. XPS studies of oxides of second- and third-row transition metals including rare earths. *J. Electron Spectrosc. Relat. Phenom.* **1980**, *20*, 25–45. [[CrossRef](#)]
43. Kasatkov, S.; Filatova, E.; Sakhonenkov, S.; Konashuk, A.; Makarov, A. Relationship between Ta Oxidation state and Its Local Atomic Coordination Symmetry in a Wide Range of Oxygen Non-stoichiometry Extent of TaOx. *J. Phys. Chem. C* **2019**, *123*, 6849–6860. [[CrossRef](#)]

**Disclaimer/Publisher’s Note:** The statements, opinions and data contained in all publications are solely those of the individual author(s) and contributor(s) and not of MDPI and/or the editor(s). MDPI and/or the editor(s) disclaim responsibility for any injury to people or property resulting from any ideas, methods, instructions or products referred to in the content.